



Farnsworth, A., Lunt, D., O'Brien, C., Foster, G., Inglis, G., Markwick, P., ...  
Robinson, S. A. (2019). Climate sensitivity on geological timescales  
controlled by nonlinear feedbacks and ocean circulation. *Geophysical  
Research Letters*. <https://doi.org/10.1029/2019GL083574>

Peer reviewed version

Link to published version (if available):  
[10.1029/2019GL083574](https://doi.org/10.1029/2019GL083574)

[Link to publication record in Explore Bristol Research](#)  
PDF-document

## **University of Bristol - Explore Bristol Research**

### **General rights**

This document is made available in accordance with publisher policies. Please cite only the published version using the reference above. Full terms of use are available:  
<http://www.bristol.ac.uk/pure/about/ebr-terms>

# Supporting Information for “Climate sensitivity on geological timescales controlled by non-linear feedbacks and ocean circulation”

A. Farnsworth<sup>1</sup>, D. J. Lunt<sup>1</sup>, C. O’Brien<sup>2</sup>, G. L. Foster<sup>3</sup>, G. N. Inglis<sup>4</sup>, P.

Markwick<sup>5</sup>, R. D. Pancost<sup>4</sup>, S. A. Robinson<sup>6</sup>

<sup>1</sup>School of Geographical Sciences and Cabot Institute, University of Bristol, UK

<sup>2</sup>Department of Geology and Geophysics, Yale University, USA

<sup>3</sup>Ocean and Earth Science, University of Southampton, UK

<sup>4</sup>School of Earth Sciences, School of Chemistry, and Cabot Institute, University of Bristol, UK

<sup>5</sup>Knowing Earth Ltd, UK

<sup>6</sup>Department of Earth Sciences, University of Oxford, UK

## Contents of this file

1. Figures S1 to S11

2. Table S1

## Introduction

This Supporting Information consists of Supporting Figures S1 to S11 and their captions, and references for the captions.

## References

- Cramwinckel, M. J., Huber, M., I. J. K., Agnini, C., Bijl, P. K., Bohaty, S. M., ...
- Sluijs, A. (2018). Synchronous tropical and polar temperature evolution in the eocene. *Nature*, 559, 382-386.
- Gregory, J. M., W. J. Ingram, W. J., Palmer, M. A., Jones, G. S., Stott, P. A., Thorpe, R. B., ... Williams, K. D. (2004). A new method for diagnosing radiative forcing and climate sensitivit. *Geophysical Research Letters*, 31, L03205. doi: 10.1029/2003gl018747
- Heinemann, M., Jungclaus, J. H., & Marotzke, J. (2009). Warm Paleocene/Eocene climate as simulated in ECHAM5/MPI-OM. *Climate of the Past*, 5, 785-802.
- Huber, M., & Caballero, R. (2011). The early eocene equable climate problem revisited. *Climate of the Past*, 7, 603-633.
- Kim, J.-H., Meer, J. V. D., Schouten, S., Helmke, P., Willmott, V., Sangiorgi, F., ... Damsté, J. S. S. (2010). New indices and calibrations derived from the distribution of crenarchaeal isoprenoid tetraether lipids: Implications for past sea surface temperature reconstructions. *Geochimica et Cosmochimica Acta*, 74, 4639-4654.
- O'Brien, C. L., Robinson, S. A., Pancost, R. D., Damst, J. S. S., Schouten, S., Lunt, D. J., ... Wrobel, N. E. (2017). Cretaceous sea-surface temperature evolution: Constraints from tex86 and planktonic foraminiferal oxygen isotopes. *Earth Science Reviews*, 172, 224-247.

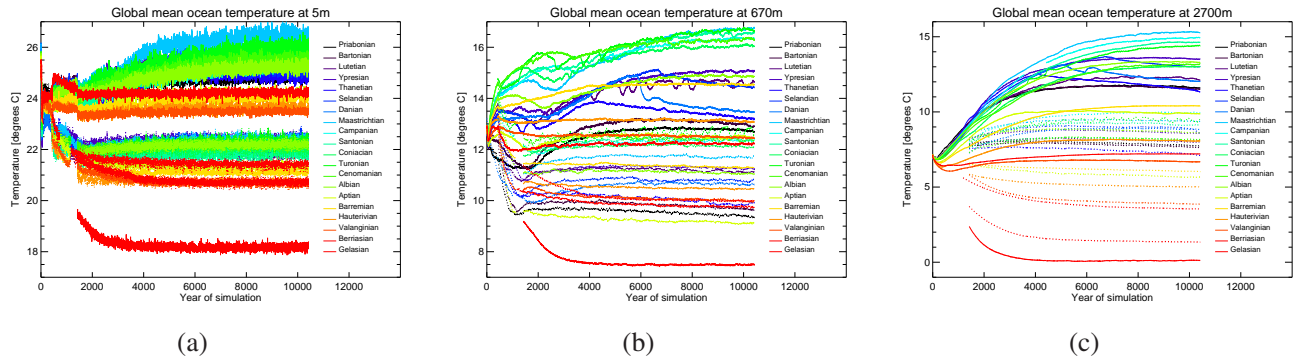


**Figure S1.** Timeseries of global mean ocean temperature over the 10,422 years of model simulations, for each geological stage and at  $\times 2$  (dotted lines),  $\times 4$  (solid lines), and  $\times 1$  CO<sub>2</sub> (Gelasian, red line) at depths of (a) 5 metres (i.e. SST); (b) 670 m; and (c) 2.7 km. This illustrates that the ocean is well equilibrated by the end of the simulations. Some of the data in the first 1500 years was not correctly archived and so does not appear.

May 10, 2019, 5:50am

**Table S1.** Modelled global mean surface temperatures (GMST) in the Cretaceous, Paleocene and Eocene  $\times 4$  and  $\times 2$  simulations.

Time period	GMST $\times 4$ [°C]	GMST $\times 2$ [°C]
Priabonian	22.24	18.44
Bartonian	22.74	18.57
Lutetian	22.89	18.19
Ypresian	23.31	18.80
Thanetian	22.19	18.24
Selandian	22.40	18.70
Danian	22.52	18.38
Maastrichtian	23.98	18.69
Campanian	22.76	18.20
Santonian	22.91	18.16
Coniacian	22.87	18.31
Turonian	23.48	18.92
Cenomanian	22.88	18.64
Albian	22.58	18.52
Aptian	21.32	17.46
Barremian	21.29	17.38
Hauterivian	21.34	17.42
Valanginian	21.03	17.28
Berriasian	21.91	18.25

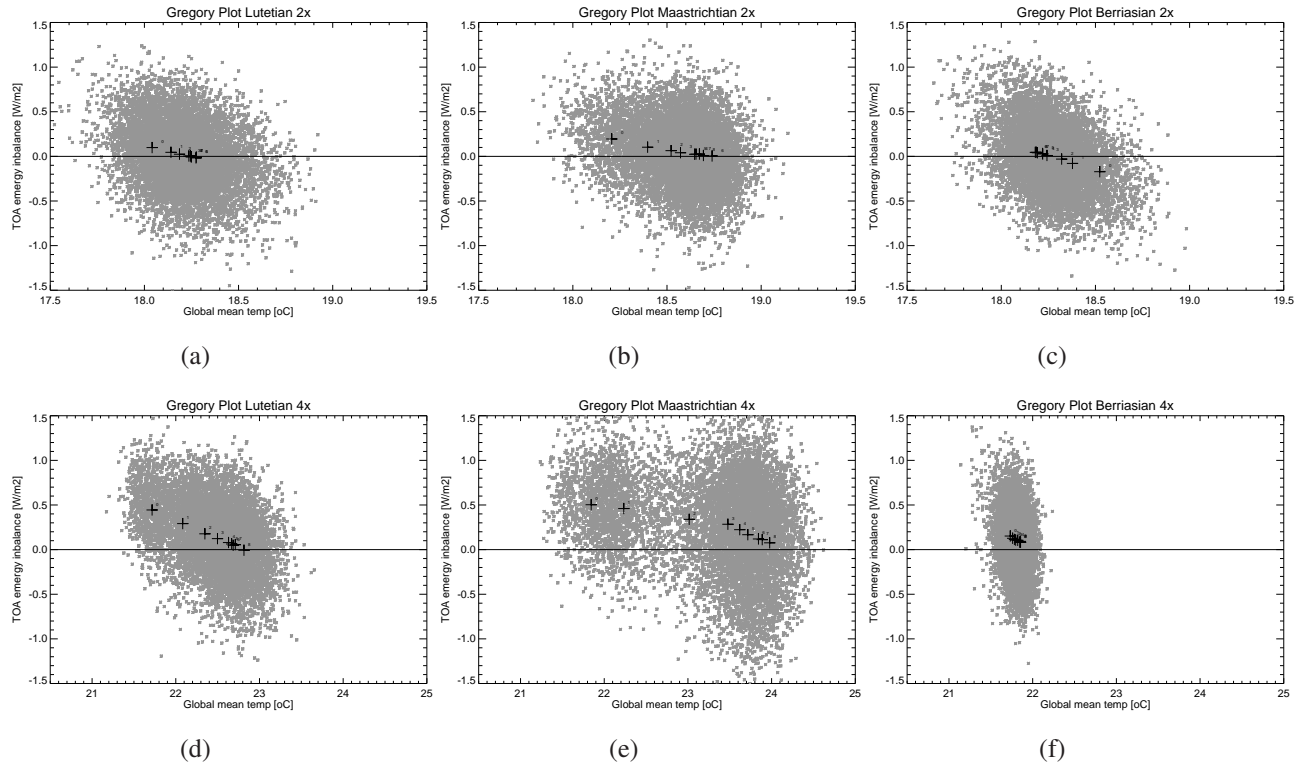


**Figure S2.** Example Gregory plots (Gregory et al., 2004) for the (a,d) Lutetian, (b,e) Maastrichtian, and (c,f) Berriaskan stages, at (a,b,c)  $\times 2$  and (d,e,f)  $\times 4$  CO<sub>2</sub>. x-axis is global mean surface temperature [°C] and y-axis is the net top-of-the-atmosphere global mean energy flux [Wm<sup>-2</sup>]. Each grey dot represents a single year of the last 9,000 years of simulations, and black crosses show averages of each of the 9 millennia. All simulations are approaching equilibrium (zero on the y axis) over time, and there are some interesting shifts in state, for example as seen by the two distinct ‘clouds’ of points in panel (e).

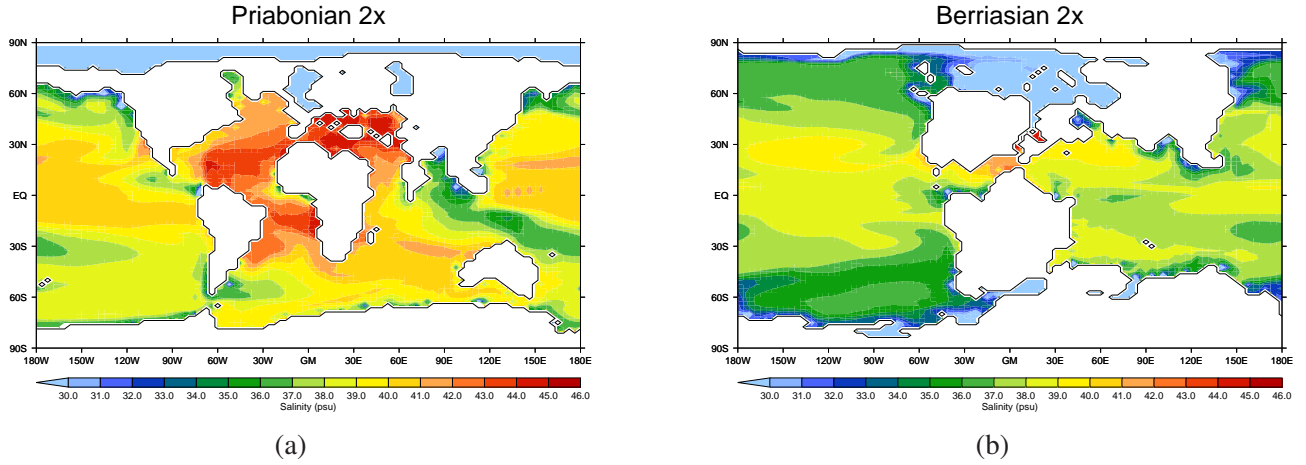


**Figure S3.** Surface salinity [psu] in the (a) Priabonian and (b) Berriasiyan  $\times 2$  simulations.

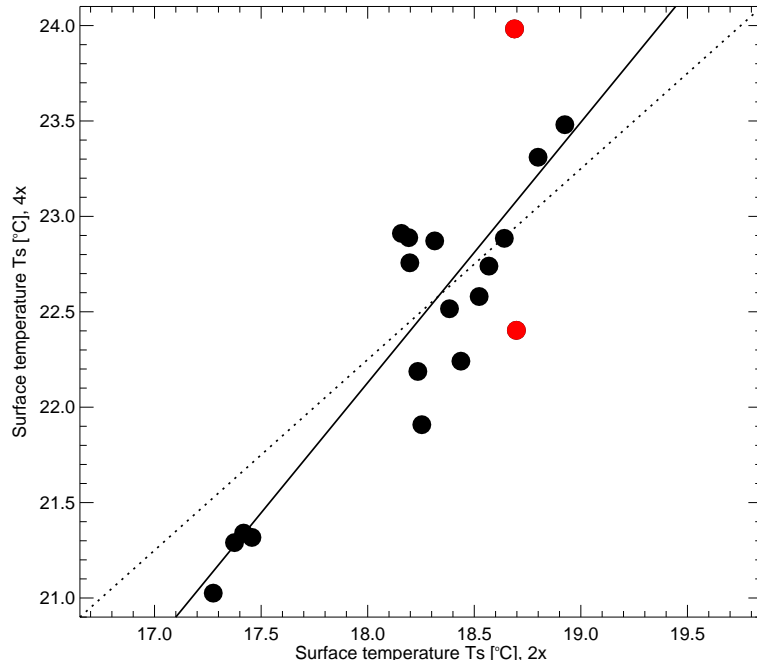


**Figure S4.** Global mean temperature in the  $\times 4$  simulations relative to the  $\times 2$  simulations.

Dotted line with a unity gradient shows a constant climate sensitivity of  $3.35^{\circ}\text{C}$ . Solid line shows the line of best fit. Red points are the Maastrichtian and Selandian which exhibit a switch in ocean circulation between  $\times 2$  and  $\times 4$ .

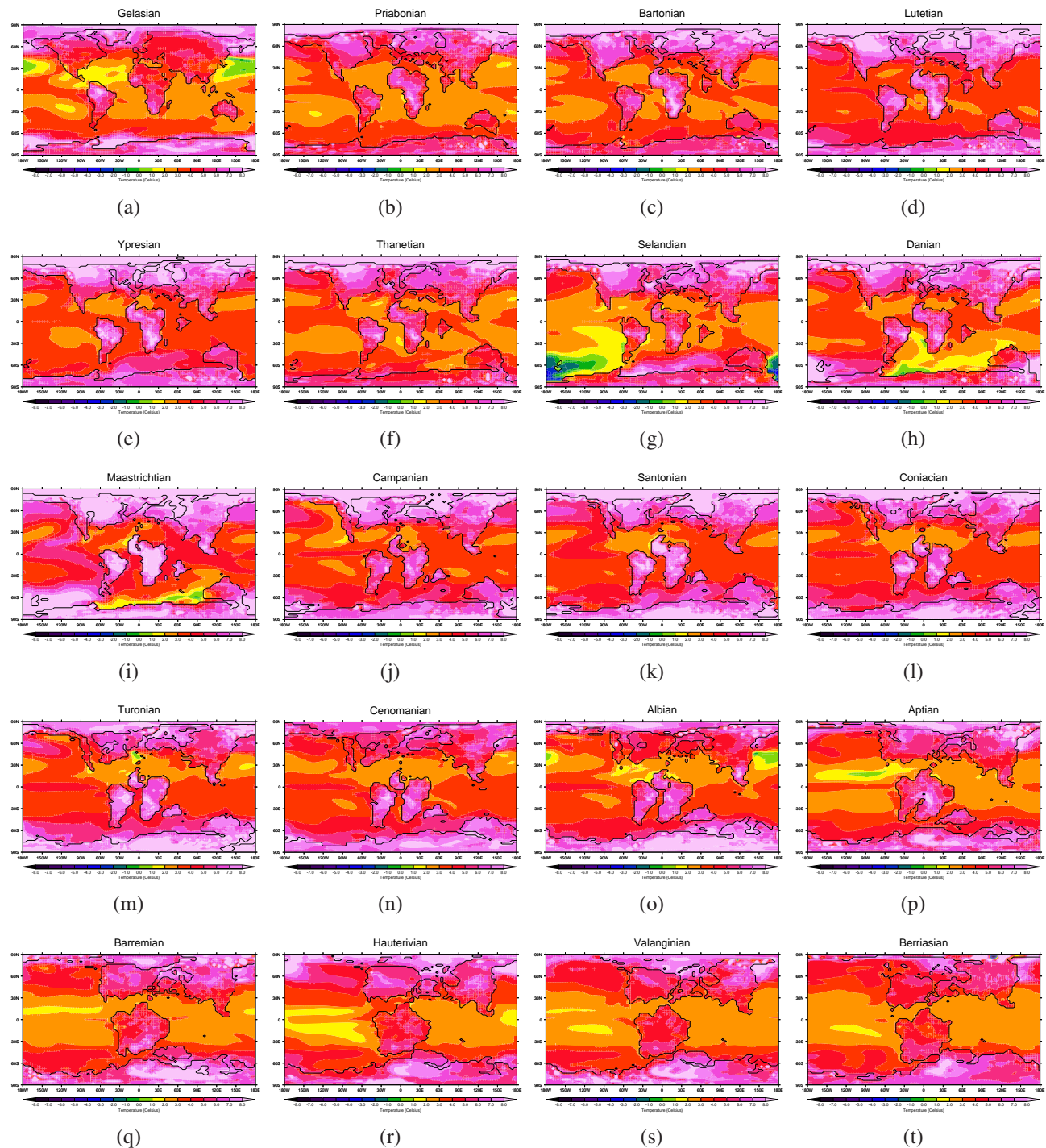


**Figure S5.** Climate sensitivity ( $\times 4 - \times 2$ ) for each time period simulated [ $^{\circ}\text{C}$ ].

May 10, 2019, 5:50am

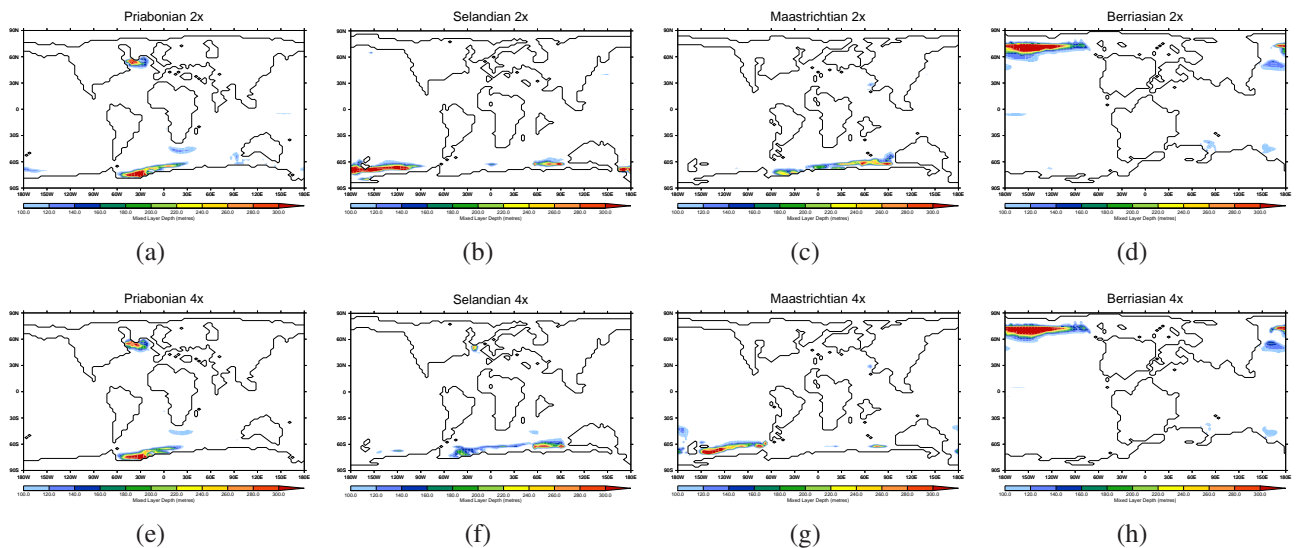


**Figure S6.** Mixed layer depth (metres) in the (a,e) Priabonian (Eocene), (b,f) Selandian (Paleocene), (c,g) Maastrichtian (Late Cretaceous), and (d,h) Berriasian (Early Cretaceous) stages, at (a,b,c,d)  $\times 2$  and (e,f,g,h)  $\times 4$  CO<sub>2</sub>.

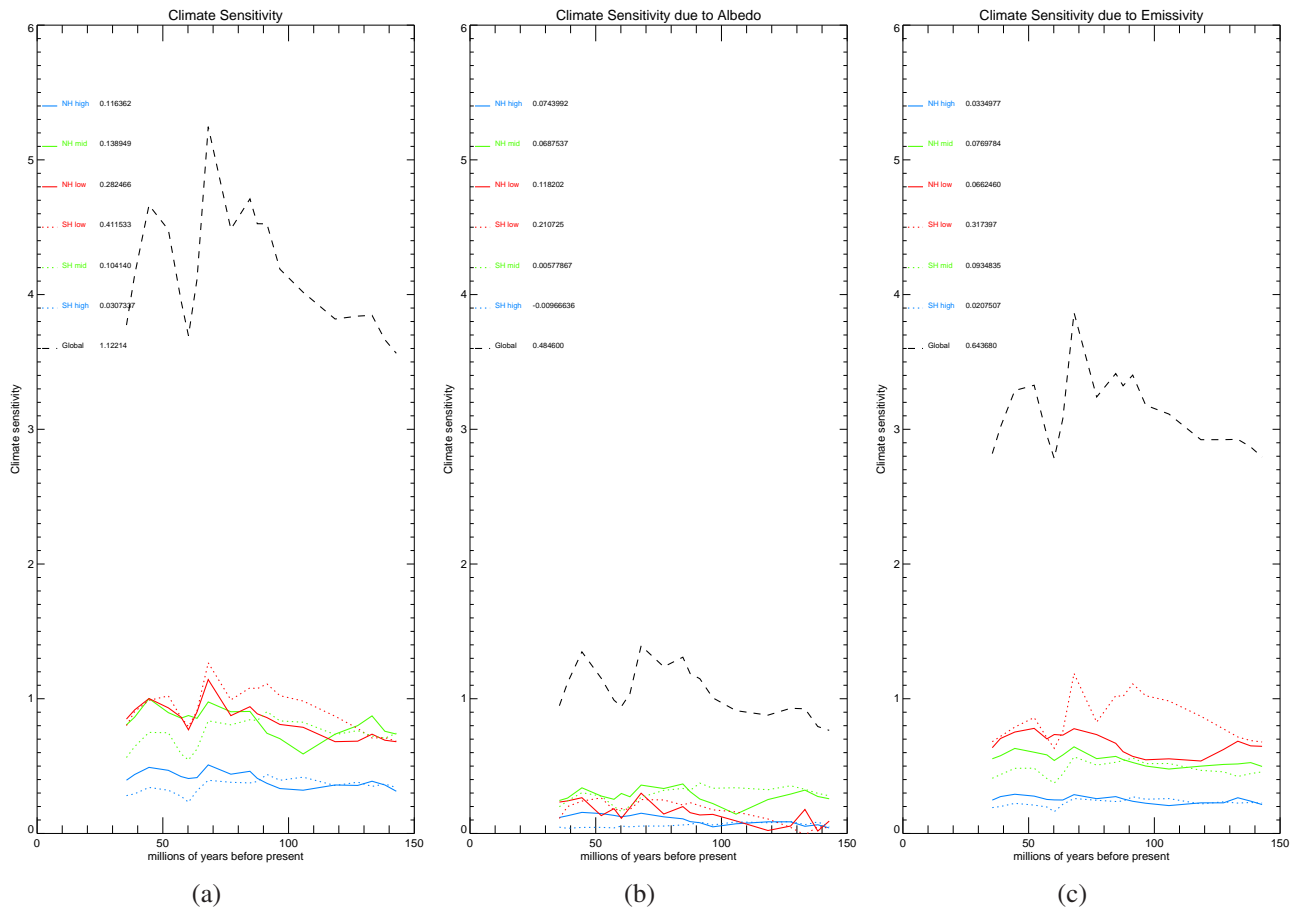


**Figure S7.** (a) Evolution of climate sensitivity (black dotted line). Coloured lines show how this evolution is partitioned between different latitudinal bands, accounting for the varying surface area of each band. The numbers in the top left give the trend through the Cretaceous for each region. (b) As (a), but showing the contribution to climate sensitivity from changes in planetary albedo, following Heinemann et al. (2009). (c) as (b), but for changes in emissivity.

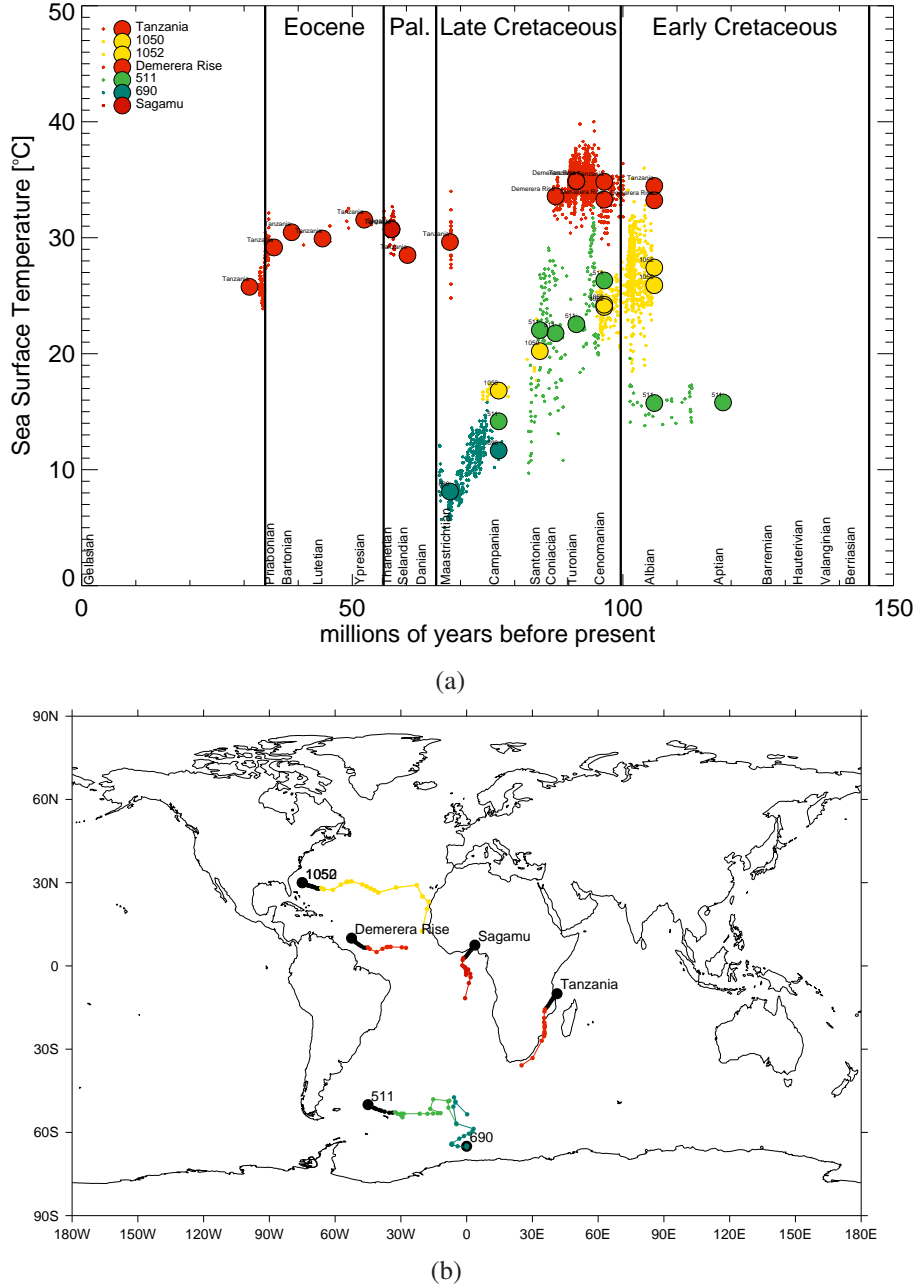


**Figure S8.** (a) Cretaceous, Paleocene, and Eocene  $\delta^{18}\text{O}$  SST compilations of O'Brien et al. (2017) and Cramwinckel et al. (2018). Individual datapoints are shown as small dots. Data averaged over site and proxy and geological stage are shown as coloured circles. The colour corresponds to the modern latitude of each site, with warm colours for low latitudes and cold colours for high latitudes. (b) Locations of sites in (a). Large black dots represent the modern location. Small black dots represent the location at each Stage since the earliest Eocene, and coloured dots represent the location at each Stage during the Cretaceous to Eocene, for those Stages that the modern ocean crust was present in the paleorotations.

May 10, 2019, 5:50am

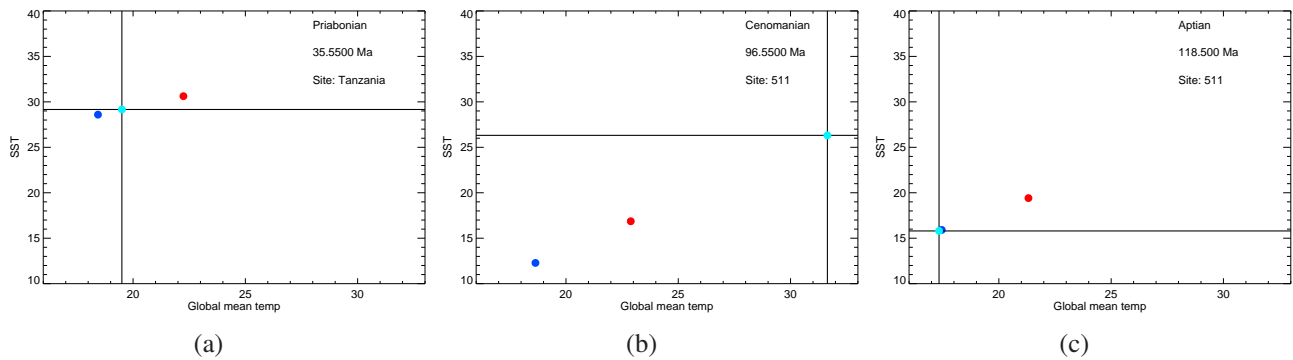


**Figure S9.** An illustration of Equation 4 in the main paper for 3 sites: (a) Tanzania in the Priabonian; (b) Site 511 in the Cenomanian; (c) Site 511 in the Aptian. The vertical line shows  $\langle T \rangle^{inferred}$  and the horizontal line shows  $T^{proxy}$ , which intercept at the light blue dot. The dark blue dot shows  $T^{2x}$  and  $\langle T^{2x} \rangle$ , and the red dot shows  $T^{4x}$  and  $\langle T^{4x} \rangle$ . The Cenomanian site is found by extrapolation substantially outside the range of the model simulations and is therefore more uncertain than the others.

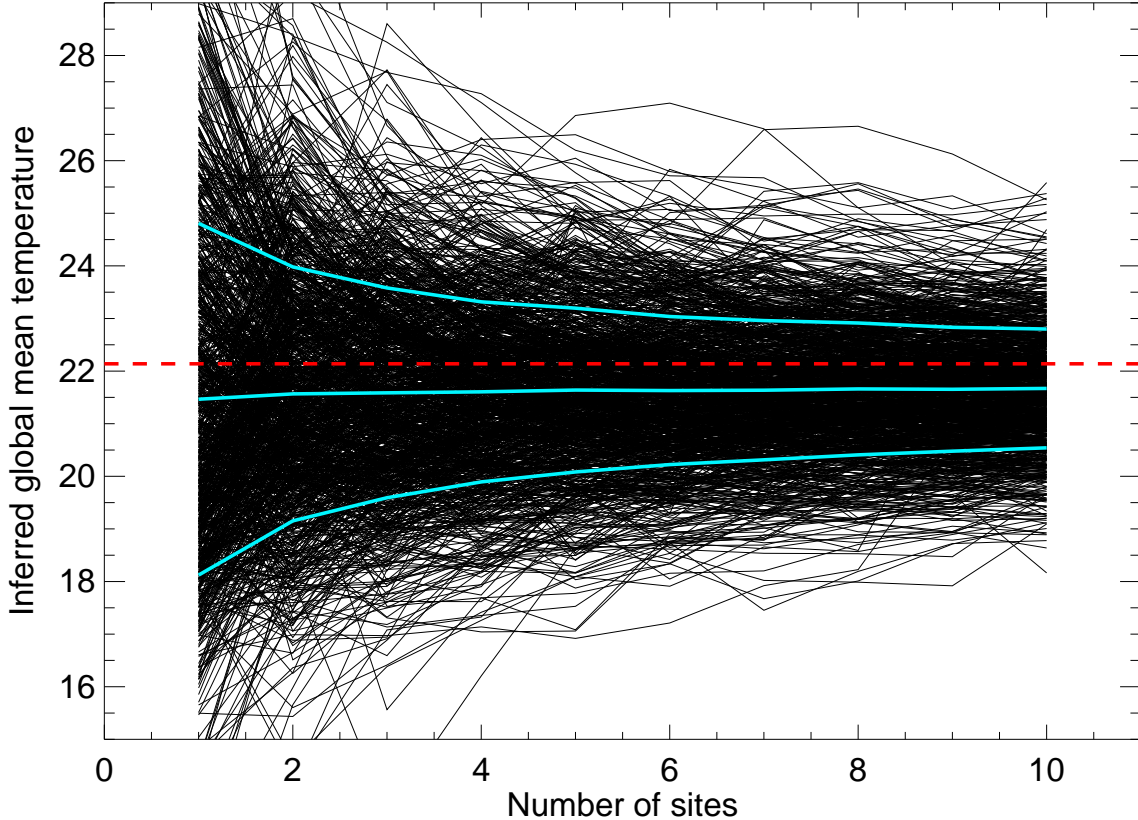


**Figure S10.** Uncertainty analysis for estimate of global mean temperatures. In order to estimate the uncertainty in our inferred global mean temperatures, we take an existing early Eocene simulation produced by a different model (Huber & Caballero, 2011), for which we calculate the true global mean surface temperature (red dashed line). We then generate synthetic paleo data from this simulation, at random sites over the globe. We then calculate the error in our method for estimating global mean temperature, given 1,2,3,... up to 10 synthetic proxy sites over the globe. We did this multiple (1000) times with different sets of random sites (black lines). Central blue line shows the mean reconstructed global mean temperature as a function of number of sites. Outer blue lines show plus and minus one standard deviation. The standard deviations are shown as vertical orange bars in Figure 2 in the main paper, according to the number of sites.

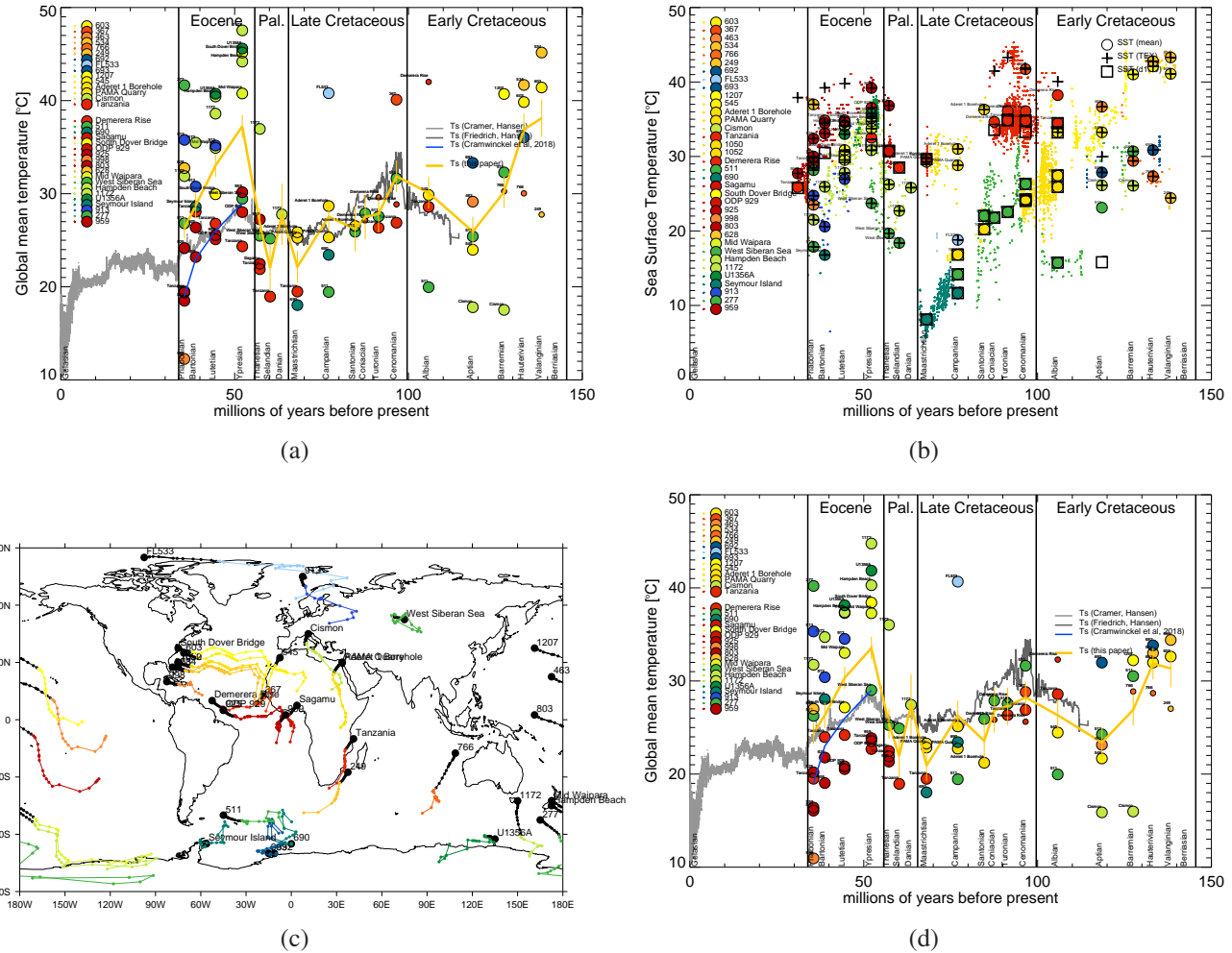


**Figure S11.** (a) As Figure 2 in the main paper, but including estimates from  $\text{TEX}_{86}$  in addition to  $\delta^{18}\text{O}$ . (b) As Figure S8(a), but including estimates from  $\text{TEX}_{86}$  in addition to  $\delta^{18}\text{O}$ . The plusses show data averaged over just  $\text{TEX}_{86}$ , and squares show data averaged over just  $\delta^{18}\text{O}$ . (c) As Figure S8(b), but including sites with  $\text{TEX}_{86}$  in addition to  $\delta^{18}\text{O}$ . (d) as (a) but for an exponential calibration (Kim et al., 2010) instead of the linear  $\text{TEX}_{86}$  calibration.